

Pt Magnetic Polarization on $Y_3Fe_5O_{12}$ and Magnetotransport Characteristics

Y. M. Lu,¹ Y. Choi,² C. M. Ortega,³ X. M. Cheng,⁴ J. W. Cai,^{1,*} S. Y. Huang,⁵ L. Sun,^{3,†} and C. L. Chien⁵

¹*Beijing National Laboratory for Condensed Matter Physics, Institute of Physics, Chinese Academy of Sciences, Beijing 100190, China*

²*Advanced Photon Source, Argonne National Laboratory, Argonne, Illinois 60439, USA*

³*Department of Mechanical Engineering and Texas Center for Superconductivity (TcSUH), University of Houston, Houston, Texas 77204, USA*

⁴*Department of Physics, Bryn Mawr College, Bryn Mawr, Pennsylvania 19010, USA*

⁵*Department of Physics and Astronomy, Johns Hopkins University, Baltimore, Maryland 21218, USA*

(Received 29 December 2012; published 5 April 2013)

Thin Pt films on an yttrium iron garnet (YIG = $Y_3Fe_5O_{12}$) show ferromagneticlike transport properties, which may impact the functionality of Pt in spin current detection, but do not provide direct quantitative information on the Pt magnetization. We report magnetic x-ray magnetic circular dichroism measurements of YIG/Pt(1.5 nm) showing an average Pt moment of $0.054 \mu_B$ at 300 K and $0.076 \mu_B$ at 20 K. This observation indicates strong proximity effects and induced magnetic ordering in Pt on magnetic insulators and their contribution to the spin-related measurements should not be neglected. The transport characteristics also suggest considerable modifications in the Pt electronic structure due to magnetic ordering.

DOI: [10.1103/PhysRevLett.110.147207](https://doi.org/10.1103/PhysRevLett.110.147207)

PACS numbers: 75.70.-i, 72.25.-b, 75.47.Np

Spintronic phenomena exploit generation, manipulation, and detection of spin polarized charge carriers. Spin imbalance exists in magnetic materials where band structure splitting results in differences in effective mass, Fermi velocity, wave vector and density of states for spin-up and spin-down charge carriers [1–3]. Recently it has been demonstrated that, in addition to magnetic materials, spin imbalance can also be generated in nonmagnetic materials by an external electrical field, magnetic field or thermal gradient. Even more significantly, one can now explore the effects of a pure spin current without the accompaniment of a charge current carrying a maximal spin angular momentum with minimal charge carriers [4–7].

The spin Hall effect (SHE) is among the first pure spin current phenomena, where a charge current in a nonmagnetic material results in a pure spin current by the strong spin-orbit coupling of the host. Direct SHE has been observed in a number of nonmagnetic metals and semiconductors [1,2] and the resultant spin accumulation can be detected optically [3]. To electrically measure a pure spin current, one can use a lateral nonlocal spin valve [4,5] structure where a ferromagnetic component is placed within the spin diffusion length of only a few tens of nm from the current. In the inverse spin Hall effect [6,7], a nonmagnetic metal with strong spin-orbit coupling can convert a pure spin current into charge accumulation. The prowess of converting a spin current to an electrical signal via the inverse spin Hall effect is specified by the spin Hall angle Θ_H [8,9], which is the ratio of the spin Hall conductivity and the charge conductivity. As in the case of its counterpart of charge Hall angle, the value of Θ_H can be of either sign. A number of metals with a large Θ_H have

been measured experimentally. Some experimental values of Θ_H are consistent with calculated results, whereas others disagree even in sign.

Of all the nonmagnetic metals, platinum (Pt) has been used most often as a pure spin current detector. Indeed, Pt is instrumental in establishing virtually all the pure spin current phenomena including the spin Seebeck effect (SSE) [10,11], spin pumping [12], spin Hall switching [13], and spin Hall induced ferromagnetic resonance [14]. In all of these cases there are magnetically ordered and nonmagnetic (Pt) interfaces in generating, transporting, and detecting the spin currents. It is essential to determine if the nonmagnetic metal in contact with a ferromagnetic material acquires ferromagnetic characteristics, or its unique role in converting pure spin current would be compromised. Thus, it is of critical importance to ascertain the nonmagnetic nature of spin current detectors, such as Pt, so that the magneto- and thermo- spin transport phenomena can be unequivocally established.

Recently, SSE in ferromagnetic insulators in the longitudinal geometry has been studied in detail [15,16]. Since in this geometry the temperature gradient is along the spin current direction, one expects there should only be SSE without the presence of the anomalous Nernst effect, which contaminates the SSE in the transverse geometry. However, the YIG/Pt samples, where a Pt thin film has been grown on an insulating ferrimagnetic $Y_3Fe_5O_{12}$ (YIG), unexpectedly show anisotropic magnetoresistance (AMR), anomalous Hall effect (AHE), and anomalous Nernst effect behaviors. These ferromagneticlike characteristics strongly suggest the presence of induced Pt magnetic moments, and from the Pt thickness dependence,

Pt moments close to the YIG/Pt interface. However, these acute magnetic proximity effects notwithstanding, magnetotransport results do not provide direct and quantitative information on the Pt magnetization.

In this work, we report on direct Pt magnetic moment measurements using x-ray magnetic circular dichroism (XMCD). XMCD is an element specific technique that determines the induced magnetic moments in the Pt atoms. XMCD has been used previously to reveal Pt moments in contact with various conducting ferromagnetic surfaces and confirming the interfacial proximity behavior [17–19]. In the present case, we have observed clear temperature dependent ferromagnetic ordering in the Pt thin films grown on epitaxial YIG substrates. This observation provides direct evidence of the induced moment in Pt when it is in contact with magnetically ordered materials, either conducting (e.g., Fe, Co) as previously established or insulating (e.g., YIG) as reported here. The observed magnetic polarization in Pt due to the proximity effect when in contact with a ferromagnetic metal or insulator questions the suitability of Pt as a pure spin current detector.

In this study, we used substrates that consist of 18 μm thick single crystalline (111) YIG layers grown by liquid phase epitaxy on (111) $\text{Gd}_3\text{Ga}_5\text{O}_{12}$ (GGG) substrates. The YIG layers have a top surface root mean square roughness of less than 0.3 nm over a scanning area of $1 \times 1 \mu\text{m}^2$, as characterized by atomic force microscopy [Fig. 1(a)]. Full width at half maximum of the (444) peak rocking curve from these YIG is about 0.0116° , as measured on a Bruker D8 Discover x-ray diffractometer using $\text{Cu } K\alpha_1$ radiation. Patterned Pt thin films with thickness between 1.3 and 30 nm via a physical mask were sputter deposited on GGG/YIG samples. The samples for x-ray diffraction, XMCD, and transport measurements have the dimension of $5 \times 3 \times 0.5 \text{ mm}^3$. To establish the close relationship between XMCD and the magneto- and thermal transport properties, specimens cut from the same sample have been used in various measurements.

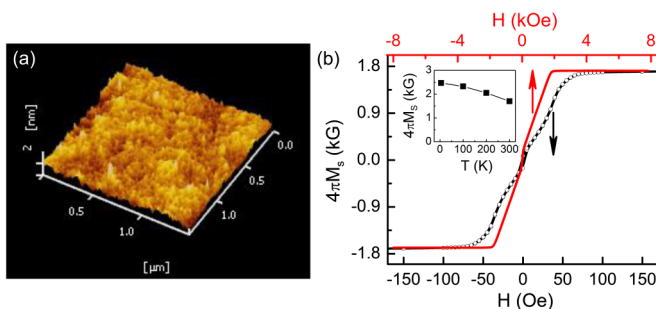


FIG. 1 (color online). (a) Atomic force microscopy surface topography of a representative YIG film and (b) corresponding room temperature in-plane and perpendicular M - H curves. The inset shows the temperature dependence of the YIG spontaneous magnetization.

Magnetic hysteresis loop measurements performed on a Quantum Design superconducting quantum interference device magnetometer show that the YIG films are magnetically soft and isotropic in the film plane. As shown in Fig. 1(b), at room temperature, the YIG layer has an in-plane saturation field of about 60 Oe and a spontaneous magnetization ($4\pi M_S$) of 1.75 kG, which is revealed in the out-of-plane measurements due to the shape anisotropy. As shown in the inset of Fig. 1(b), the spontaneous magnetization of YIG increases monotonically with decreasing temperature and reaches 2.48 kG at 5 K. These magnetic properties agree well with those of bulk YIG.

XMCD measurements were performed on the 4ID-D beam line at the Advanced Photon Source at the Argonne National Laboratory using the fluorescence detection mode at the Pt $L_{2,3}$ absorption edges ($2p_{1/2,3/2} \rightarrow 5d$ transition). Circularly polarized x rays were generated using a 500 μm -thick diamond phase retarder, and XMCD was measured by switching the x-ray helicity. An electromagnet was used to generate external magnetic fields parallel to the sample surface and in the plane determined by the incident x-ray direction and the sample surface normal direction. The x-ray incident angle is about 3° .

XMCD can provide direct magnetization measurement along the wave vector direction with element specificity. An XMCD characterization of Pt L_2 and L_3 edges was performed to probe the magnetization of Pt atoms on YIG. Contrary to the report by Geprags *et al.* [20], a clear XMCD signal from Pt has been detected. Figure 2 shows the polarization-averaged x-ray adsorption spectra (XAS) and XMCD spectra for a 1.5 nm Pt film. The same scaling factor to normalize the XAS step height to 2.07 at the L_3 edge and 1.00 at the L_2 edge was used for the XMCD spectra [21]. The clear dichroism effect can be observed and the sign of the XMCD spectra changes with applied magnetic field direction. Also the XMCD signal intensifies when measurement temperature is lowered from 300 to 20 K. Inset of Fig. 2(b) confirms that the XMCD signal is not experimental artifact such as a result of energy shifts between two circular polarizations. Statistical errors in the XMCD signal are shown in the inset.

The Pt L_3 XMCD-to-XAS step edge height ratio is around 1% for this sample. This value is significantly lower than XMCD signals observed from Pt in contact with pure $3d$ ferromagnets. In comparison, in FePt nanoparticles, a 15% XMCD to XAS step edge height ratio was observed at the Pt L_3 [22]. For thin film structures, a 22% XMCD to XAS step edge height ratio was observed for a 0.15 nm Pt grown on Co. This ratio decreases to about 9% and 4% when the Pt thickness has been increased to 1 and 2 nm, respectively. Assuming the Pt magnetization possesses an exponential decay from the Pt/Co interface, a decaying constant of 0.41 nm was reported [21]. Resonant magnetic x-ray reflectivity studied further suggested that the induced Pt moments are located within 1 nm from the Co/Pt

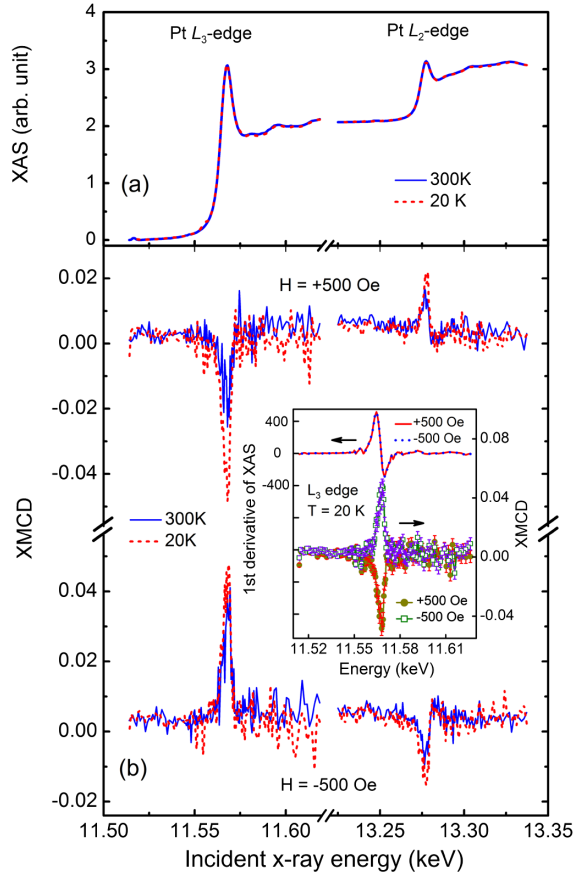


FIG. 2 (color online). (a) Normalized synchrotron x-ray absorption spectra, and (b) corresponding x-ray magnetic dichroism with an in-plane magnetic field of ± 500 Oe from the YIG/Pt(1.5 nm) at 300 and 20 K. Inset compares the first derivative of the XAS spectra with the XMCD signal of L_3 edge obtained at 20 K. Error bars are included in the XMCD results to indicate measurement noise level.

interface [21]. In Ni/Pt multilayers, a layer-resolved XMCD study confirmed that the induced Pt moment was localized near the Ni/Pt interfaces [19]. The lower value of the observed XMCD signal strength from Pt grown on YIG is a direct reflection of the smaller magnetization in YIG.

Further investigation using the sum rules [23,24] allows the determination of per Pt atom orbital moment m_o and spin asymmetry term $m_s + 7m_T$, including the spin moment m_s and the magnetic dipole moment m_T . We used the number of $5d$ holes of $n_h^{\text{Pt}} = 1.73$ as done for FePt [22]. For the two measurement temperatures of 300 and 20 K, m_o has been determined to be $0.010 \mu_B$ and $0.017 \mu_B$, and the effective spin moment $m_s + 7m_T$ has been determined to be $0.044 \mu_B$ and $0.059 \mu_B$, respectively. In Co/Pt bilayers, the $7m_T$ term was about 1 order of magnitude smaller [21]. An increase of average Pt moment from $0.054 \mu_B$ at 300 K to $0.076 \mu_B$ at 20 K is recorded as the YIG magnetization changes from 1.75 to 2.48 kG. The fast increase in Pt moment could reflect the significant magnetization change in YIG.

In addition to XMCD, it is essential to compare the resistivity, MR, thermogalvanic as well as the Hall effect for Pt thin films grown on YIG and GGG substrates. AMR effects can be clearly observed in the Pt films grown on YIG. Figure 3 shows the representative geometry and thickness dependences of the MR and thermal effects in these samples. Such effects are absent from the GGG/Pt samples. The longitudinal and transverse MR of the YIG/Pt show the same field dependences as those of the hysteresis loops of YIG. Coupled with the AMR effect the anomalous Nernst effect as shown in Figs. 3(b) and 3(c) gives the thermovoltage measured for YIG/Pt (4 nm) with a temperature gradient applied perpendicular to the sample plane. The field dependence of the thermal voltage coincides with the sample AMR, both coupled to the magnetization of the film.

With the in-plane applied magnetic field exceeding the saturation field of YIG and rotating in plane, the resistivity shows a $\cos^2\theta$ dependence, where θ is the angle between the field direction and the length direction of the Pt pattern [inset of Fig. 3(a)]. A decrease in MR ratio with increasing film thickness [Fig. 3(d)] supports the argument that

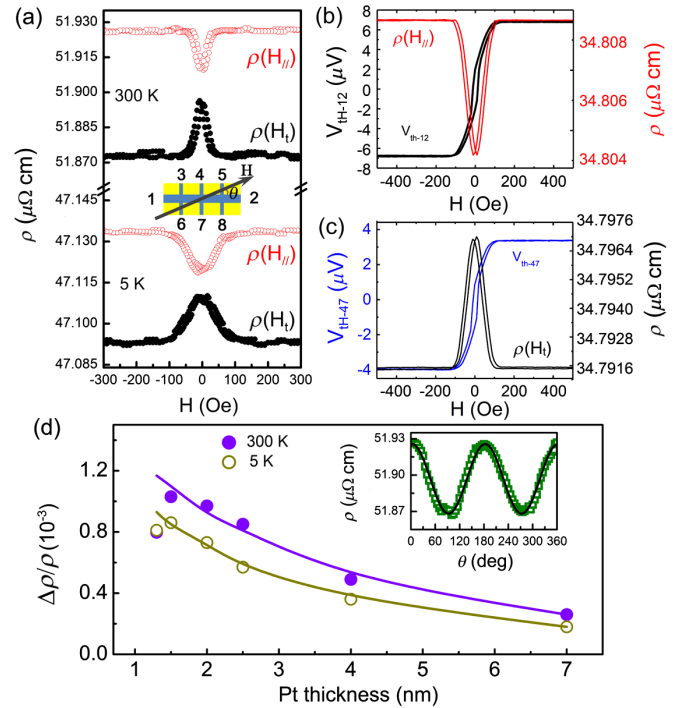


FIG. 3 (color online). (a) Longitudinal and transverse MR curves of a YIG/Pt(1.5 nm) sample measured at 300 and 5 K with electrode configuration shown in the inset; (b) and (c) coupled MR and Nernst effect measurements for a YIG/Pt(4.0 nm) sample; and (d) Pt thickness dependence of AMR ratio for YIG/Pt at 300 and 5 K. The solid lines are guides for the eye. Inset in (d) plots the resistivity as a function of in-plane field direction (8 kOe) for a representative sample YIG/Pt(1.5 nm) at 300 K, and the solid line is a fitting result using cosine square function.

magnetic order in Pt deposited on YIG can be a result of the magnetic proximity effect.

A closer look at the temperature dependence of the magnetotransport properties of the Pt thin films shows different characteristics from conventional bulk ferromagnetic materials; i.e., the magnetoresistance has an initial increase with decreasing temperature from room temperature, but the trend turns negative below 100 K [Fig. 4(a)]. In addition, resistivity of the Pt thin film samples also shows significant thickness dependence. For films thicker than 10 nm, sample resistivity decreases gradually with temperature reduction. But nonmonotonic temperature dependence becomes obvious when film thickness drops below 4 nm. As shown in Fig. 4(b), a resistivity minimum appears at around 20 K for the 1.5 nm Pt, 15 K for the 2 nm Pt, and 10 K for 4 nm Pt, respectively. This occurrence of the metal to insulator transition in the Pt thin film sample should originate from the weak localization of electrons caused by dimensional effect. In any case, the slight resistivity increase for thin Pt layers at low temperature cannot account for the AMR reduction below 100 K.

The Pt film resistivity grown on GGG and YIG is compared. As shown in Fig. 4(b), both series samples exhibit very similar thickness and temperature dependence. But under otherwise same conditions, GGG/Pt shows a larger resistivity and this becomes more significant for thinner Pt layers. Considering the fact that the YIG underlayer and the GGG substrates have the same surface roughness, the resistivity reduction of the Pt layers should not come from the thin film uniformity. The introduction of magnetic ordering in Pt by the YIG underlayer will result in the band split for the Pt *5d* spin-up and spin-down electrons, which in turn will lower the density of states

(DOS) at the Pt Fermi level. Reduction in the DOS will result in less *s-d* scattering and lead to a smaller resistivity for the magnetic ordered Pt layer. Therefore, comparison between the Pt film resistivity of YIG/Pt and GGG/Pt also suggests that the electronic structure of the Pt layer has been appreciably modified by the YIG underlayer.

Besides AMR, the YIG/Pt samples possess both temperature-sensitive ordinary (OHE) and anomalous (AHE) Hall effect. Since the temperature dependence of AHE in the YIG/Pt films has been discussed previously [15], we focus on the OHE in the samples. As shown in Fig. 4(c), thinner Pt layers exhibit more prominent OHE temperature dependences. There is a change of OHE coefficient sign from negative at room temperature to positive at low temperatures. Phenomenologically, the OHE coefficient (R_O) and resistivity of a material can be related to the charge carrier concentration and corresponding mobility as,

$$R_O = \frac{p\mu_p^2 - n\mu_n^2}{q(p\mu_p + n\mu_n)^2},$$

$$\rho = \frac{1}{q(n\mu_n + p\mu_p)},$$

where p , n , μ_p , and μ_n are the hole, electron density, and their mobility, respectively. With the possible existence of both charge carriers, it is impossible to determine their temperature dependences just from the OHE coefficient and resistivity data. But nonetheless, these measurements suggest that the electronic band structure can have significant change for thin Pt films and result in OHE coefficient increase and AMR reduction. Strong temperature OHE coefficient dependence can only be observed for samples on YIG substrates, not on the GGG substrates, and will diminish with increasing Pt thickness. These observations again indicate the significant interactions between YIG and Pt and the interfacial nature of this interaction. A recent *ab initio* study explained the spin polarization mechanism in Pt on YIG [25]. Phenomenologically, we believe the interfacial electrons from Pt can penetrate into YIG and be reflected back into the Pt. Affected by the strong exchange interaction within YIG, spin splitting and appreciable change in the DOS at the Fermi level will happen in the interfacial Pt layers, and, thus, lead to the observed thickness-dependent Pt transport behavior. The details of the phenomenon are currently under theoretical investigation and are not the focus of this Letter.

In summary, well-defined XMCD peaks at the *L* adsorption edges of Pt and the inversion of the dichroic signal with opposite magnetic fields, both at 300 and 20 K, demonstrate a clear magnetic polarization and proximity effect in Pt thin films grown on ferromagnetic YIG. Using XMCD, the average polarized Pt magnetization of $0.076 \mu_B$ per Pt has been determined for a layer 1.5 nm thick. Pt moment orientation and temperature dependence

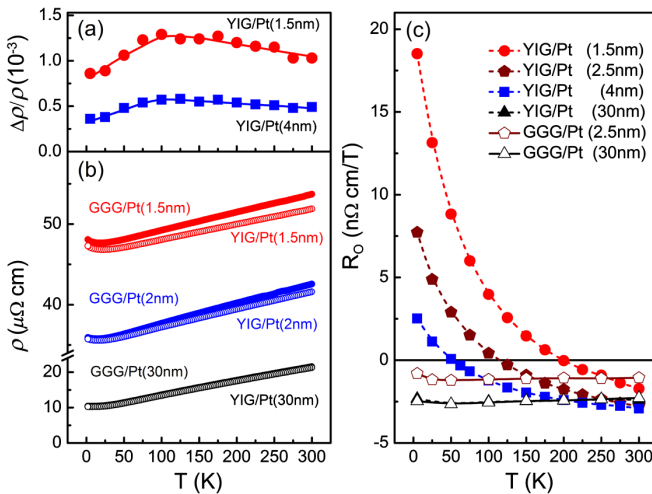


FIG. 4 (color online). (a) Temperature dependence of the anisotropic magnetoresistance for a YIG/Pt(1.5 nm) and a YIG/Pt(4 nm) film. (b) Comparison of the thickness dependent Pt thin film resistivity grown on YIG and GGG substrates as a function of temperature; and (c) ordinary Hall coefficient measured for Pt films grown on YIG and GGG substrates.

show strong correlation to the YIG magnetization. Magnetotransport properties of YIG/Pt show thickness-dependent ferromagneticlike behaviors that are absent in the GGG/Pt samples. The magnetotransport characteristics of thin Pt layers are also different from common uniform magnetic material, displaying unconventional AMR and OHE coefficient temperature dependences.

J. W. C. is in debt to Dr. X.-G. Zhang at the Oak Ridge National Laboratory and Dr. J. R. Sun at the Institute of Physics of CAS for fruitful discussions. This work was supported by the National Basic Research Program of China under Grant No. 2009CB929201, the National Natural Science Foundation of China under Grants No. 51171205, No. 51021061, and No. 50831002, and the U.S. NSF Grant No. DMR-0520491. The use of the Advanced Photon Source at the Argonne National Laboratory is supported by the U.S. DOE under Contract No. DE-AC02-06CH11357.

*jwcai@iphy.ac.cn

†Li.Sun@mail.uh.edu

- [1] M. I. D'Yakonov and V. I. Perel, *Phys. Lett.* **35A**, 459 (1971).
- [2] J. E. Hirsch, *Phys. Rev. Lett.* **83**, 1834 (1999).
- [3] Y. K. Kato, R. C. Myers, A. C. Gossard, and D. D. Awschalom, *Science* **306**, 1910 (2004).
- [4] F. J. Jedema, H. B. Heersche, A. T. Filip, J. J. A. Baselmans, and B. J. van Wees, *Nature (London)* **416**, 713 (2002).
- [5] S. O. Valenzuela and M. Tinkham, *Nature (London)* **442**, 176 (2006).
- [6] K. Ando, Y. Kajiwara, S. Takahashi, S. Maekawa, K. Takemoto, M. Takatsu, and E. Saitoh, *Phys. Rev. B* **78**, 014413 (2008).
- [7] E. Saitoh, M. Ueda, H. Miyajima, and G. Tatara, *Appl. Phys. Lett.* **88**, 182509 (2006).
- [8] N. E. Christensen, *J. Phys. F* **8**, L51 (1978).
- [9] L. Q. Liu, C. F. Pai, Y. Li, H. W. Tseng, D. C. Ralph and R. A. Buhrman, *Science* **336**, 555 (2012).
- [10] G. E. W. Bauer, E. Saitoh, and B. J. van Wees, *Nat. Mater.* **11**, 391 (2012).
- [11] K. Uchida, S. Takahashi, K. Harii, J. Ieda, W. Koshibae, K. Ando, S. Maekawa, and E. Saitoh, *Nature (London)* **455**, 778 (2008).
- [12] Y. Kajiwara, K. Harii, S. Takahashi, J. Ohe, K. Uchida, M. Mizuguchi, H. Umezawa, H. Kawai, K. Ando, K. Takanashi, S. Maekawa, and E. Saitoh, *Nature (London)* **464**, 262 (2010).
- [13] I. M. Miron, K. Garello, G. Gaudin, P. J. Zermatten, M. V. Costache, S. Auffret, S. Bandiera, B. Rodmacq, A. Schuhl, and P. Gambardella, *Nature (London)* **476**, 189 (2011).
- [14] L. Q. Liu, T. Moriyama, D. C. Ralph, and R. A. Buhrman, *Phys. Rev. Lett.* **106**, 036601 (2011).
- [15] S. Y. Huang, X. Fan, D. Qu, Y. P. Chen, W. G. Wang, J. Wu, T. Y. Chen, J. Q. Xiao, and C. L. Chien, *Phys. Rev. Lett.* **109**, 107204 (2012).
- [16] M. Weiler, M. Althammer, F. D. Czeschka, H. Huebl, M. S. Wagner, M. Opel, I.-M. Imort, G. Reiss, A. Thomas, R. Gross, and S. T. B. Goennenwein, *Phys. Rev. Lett.* **108**, 106602 (2012).
- [17] S. Rüegg, G. Schütz, P. Fischer, R. Wienke, W. B. Zeper and H. Ebert, *J. Appl. Phys.* **69**, 5655 (1991).
- [18] W. J. Antel, Jr, M. M. Schwickert, Tao Lin, W. L. O'Brien, and G. R. Harp, *Phys. Rev. B* **60**, 12933 (1999).
- [19] F. Wilhelm, P. Pouloupoulos, G. Ceballos, H. Wende, K. Baberschke, P. Srivastava, D. Benea, H. Ebert, M. Angelakeris, N. K. Flevaris, D. Niarchos, A. Rogalev, and N. B. Brookes, *Phys. Rev. Lett.* **85**, 413 (2000).
- [20] S. Geprägs, S. Meyer, S. Altmannshofer, M. Opel, F. Wilhelm, A. Rogalev, R. Gross, and S. T. B. Goennenwein, *Appl. Phys. Lett.* **101**, 262407 (2012).
- [21] M. Suzuki, H. Muraoka, Y. Inaba, H. Miyagawa, N. Kawamura, T. Shimatsu, H. Maruyanma, N. Ishimatsu, Y. Isohama, and Y. Sonobe, *Phys. Rev. B* **72**, 054430 (2005).
- [22] C. Antoniak, J. Lindner, M. Spasova, D. Sudfeld, M. Acet, M. Farle, K. Fauth, U. Wiedwald, H.-G. Boyen, P. Ziemann, F. Wilhelm, A. Rogalev, and S. Sun, *Phys. Rev. Lett.* **97**, 117201 (2006).
- [23] B. T. Thole, P. Carra, F. Sette, and G. van der Laan, *Phys. Rev. Lett.* **68**, 1943 (1992).
- [24] P. Carra, B. T. Thole, M. Altarelli, and X. Wang, *Phys. Rev. Lett.* **70**, 694 (1993).
- [25] D. Qu, S. Y. Huang, J. Hu, R. Q. Wu, and C. L. Chien, *Phys. Rev. Lett.* **110**, 067206 (2013).